REPORT

Molecular basis for GIGYF–TNRC6 complex assembly

MEGHNA SOBTI,[1,2] BENJAMIN J. MEAD,[3] ALASTAIR G. STEWART,[1,2] CÁTIA IGREJA,[4] and MARY CHRISTIE[1,2,3,5]

[1]Molecular, Structural and Computational Biology Division, The Victor Chang Cardiac Research Institute, Sydney, New South Wales 2010, Australia

[2]School of Clinical Medicine, Faculty of Medicine and Health, UNSW Sydney, New South Wales 2052, Australia

[3]School of Life and Environmental Sciences, The University of Sydney, Sydney, New South Wales 2006, Australia

[4]Department of Integrative Evolutionary Biology, Max Planck Institute for Biology, D-72076 Tübingen, Germany

ABSTRACT

The GIGYF proteins interact with 4EHP and RNA-associated proteins to elicit transcript-specific translational repression. However, the mechanism by which the GIGYF1/2–4EHP complex is recruited to its target transcripts remain unclear. Here, we report the crystal structures of the GYF domains from GIGYF1 and GIGYF2 in complex with proline-rich sequences from the miRISC-binding proteins TNRC6C and TNRC6A, respectively. The TNRC6 proline-rich motifs bind to a conserved array of aromatic residues on the surface of the GIGYF1/2 GYF domains, thereby bridging 4EHP to Argonaute–miRNA complexes. Our structures also reveal a phenylalanine residue conserved from yeast to human GYF domains that contributes to GIGYF2 thermostability. The molecular details we outline here are likely to be conserved between GIGYF1/2 and other RNA-binding proteins to elicit 4EHP-mediated repression in different biological contexts.

Keywords: gene regulation; translational repression; silencing; X-ray crystallography

INTRODUCTION

Cap-dependent translation initiation requires the assembly of eIF4F, a heterotrimeric complex comprising the RNA helicase eIF4A, the scaffold protein eIF4G, and the cap-binding protein eIF4E to the mRNA 5′ m^7GpppN cap structure. eIF4G not only bridges eIF4A and eIF4E but also recruits the preinitiation complex to capped mRNA, which in turn commences scanning and identification of the start codon (Sonenberg and Hinnebusch 2009; Jackson et al. 2010). Translation initiation can therefore be regulated by factors that modulate these interactions, such as the eIF4E-binding proteins (4E-BPs) that compete with eIF4G binding to eIF4E (Mader et al. 1995; Marcotrigiano et al. 1999), or proteins that recognize the 5′ cap structure which do not associate with eIF4G. One such cap-binding protein is 4EHP (eIF4E homologous protein, also known as eIF4E2), which prevents the assembly of the eIF4F complex on target mRNAs to prevent translation initiation (Rom et al. 1998; Joshi et al. 2004; Hernández et al. 2005). In contrast with eIF4E, 4EHP interacts with GIGYF1 (Grb10-interacting GYF protein 1) and its paralog GIGYF2 (Morita et al. 2012; Chapat et al. 2017), in a manner resembling the eIF4E–eIF4G and eIF4E–4E-BP complexes (Peter et al. 2017). Knockout of *4ehp* or *Gigyf2* in mice results in perinatal and early postnatal mortality, respectively, underscoring the importance of these proteins during development (Giovannone et al. 2009; Morita et al. 2012). Moreover, different neurodegenerative presentations are also associated with the mutation or loss of GIGYF1/2 in animals and humans including schizophrenia, autism spectrum disorders, and age-related neurodegeneration (Giovannone et al. 2009; Iossifov et al. 2014; Krumm et al. 2015; Thyme et al. 2019; Satterstrom et al. 2020).

Unlike eIF4G, which recruits the translation initiation machinery, human GIGYF proteins have been shown to associate with proteins involved with mRNA degradation (e.g., the carbon catabolite repression-negative on TATA-less [CCR4-NOT] deadenylation complex; ZFP36/tristetraprolin [TTP]), translational repression (DEAD-box RNA helicase DDX6), mRNA decapping (DDX6, PatL1), ribosome quality control (e.g., ZNF598), and miRNA-mediated silencing (e.g., TNRC6 proteins) (Ash et al. 2010; Morita

[5]**Present address:** School of Medical Sciences, The University of Sydney, Sydney, New South Wales 2006, Australia

Corresponding authors: catia.igreja@tuebingen.mpg.de, tara.christie@sydney.edu.au

Article is online at http://www.rnajournal.org/cgi/doi/10.1261/rna.079596.123. Freely available online through the *RNA* Open Access option.

et al. 2012; Fu et al. 2016; Schopp et al. 2017; Amaya Ramirez et al. 2018; Peter et al. 2019; Ruscica et al. 2019; Tollenaere et al. 2019; Mayya et al. 2021). TNR6CA (also known as GW182), TNR6CB and TNRC6C are Argonaute-binding protein scaffolds that have been implicated in mRNA degradation and translational repression of miRNA targets (Jonas and Izaurralde 2015).

Mutational analysis of zebrafish TNRC6A (*Danio rerio* TNRC6A) indicated that a highly conserved PPGL motif located within the TNRC6A silencing domain contributes to translational inhibition but does not affect deadenylation, the first step of mRNA degradation (Mishima et al. 2012). The PPGL motif is also present in the human TNRC6 proteins, as well as TNRC6/GW182 proteins in other organisms, suggesting that this motif might play a conserved role in TNRC6/GW182-mediated translational repression across metazoa (Mishima et al. 2012; Moran et al. 2013). A direct interaction has been observed between TNRC6A and a fragment of GIGYF2 that encompasses its central GYF domain (Schopp et al. 2017). Knockdown of GIGYF2 affects miRNA-mediated translational repression of an mRNA reporter (Schopp et al. 2017). Furthermore, tethering assays using a TNRC6A fragment comprising the C-terminal silencing domain (Fig. 1A) indicates that the PPGL motif contributes to the silencing activity of the protein in cells (Zou et al. 2022). These results indicate that GIGYF2 is a regulator of the Argonaute–miRNA silencing complex (miRISC) activity.

The human GIGYF proteins were named after their GYF adaptor domains which recognize proline-rich sequences (PRSs) conforming to the PPGΦ consensus (where Φ corresponds to a hydrophobic residue, except for tryptophan) (Kofler et al. 2005; Ash et al. 2010). The GYF domain takes its name from a conserved glycine-tyrosine-phenylalanine (GYF) motif that is part of the larger GFP-X_4-[M/V/I]-X_2-W-X_3-GYF signature characteristic of the PRS-binding region. This hallmark of GYF domains forms a bulge-helix-bulge structural element that generates a hydrophobic ligand-binding surface (Freund et al. 1999). GYF domains can be further divided into two subfamilies that are named after the proteins from which they were first identified: the splicing factor CD2BP2 (CD2 antigen cytoplasmic tail-binding protein 2) (Nishizawa et al. 1998), and *Saccharomyces cerevisiae* (*Sc*) Smy2 (Kofler et al. 2005), which is thought to be the GIGYF2 homolog in yeast. The two subfamilies are distinguished by the length of the β1–β2 loop, as well as by the residue located at position 8 of the GYF domain; a longer β1–β2 loop and a Trp at position 8 is characteristic of the CD2BP2 family, while a shorter β1–β2 loop and an Asp at position 8 typifies the Smy2 class of GYF domains (Kofler and Freund 2006). Only three GYF domain-containing proteins are encoded in the human genome, namely, CD2BP2, GIGYF1, and GIGYF2.

The specificity of 4EHP-mediated translational repression is thought to be imparted by the GYF domain of the GIGYF proteins, which acts as an adaptor to bridge RNA-binding proteins to 4EHP (Morita et al. 2012; Fu et al. 2016; Schopp et al. 2017; Weber et al. 2020). Mutations that prevent TTP from binding to the GIGYF2 GYF domain impair TTP-mediated repression in mammalian cells (Fu et al. 2016; Peter et al. 2019). Moreover, the repression activity of zebrafish TNRC6A/GW182 can be reduced by mutation of the conserved PPGL motif (Mishima et al. 2012). Mutations within the GIGYF GYF domains that prevent interaction with PPGΦ-containing sequences correspondingly disrupt their recruitment to endogenous mRNA targets (Weber et al. 2020). The importance of the GIGYF GYF domain is further illustrated in tethering assays whereby the isolated GIGYF2 GYF domain displays repressive activity comparable to that of the full-length protein (Amaya Ramirez et al. 2018).

To understand the mechanism by which PPGΦ-containing proteins are recruited by the GIGYF–4EHP complex, we determined the crystal structures of GIGYF1 and GIGYF2 GYF domains in complex with PPGL peptides from TNRC6C and TNRC6A, respectively. These structures highlight the conserved molecular mechanism of PRS recognition by GYF domains and reveal a structural feature in metazoan GYF adaptors that contributes to domain stability.

RESULTS AND DISCUSSION

PPGΦ sequences can directly interact with the isolated GIGYF2 GYF domain

Recent work has detected a direct interaction between the C-terminal silencing domain of TNRC6C that encodes a PPGΦ motif (1369–1690; Fig. 1A) and a central portion of GIGYF2 that encompasses the GYF domain (residues 532–740; Fig. 1A; Schopp et al. 2017). The interaction was diminished when the PPGL motif was mutated and when the GYF domain was deleted (residues 607–740 of GIGYF2) (Schopp et al. 2017). We therefore examined whether the GIGYF2 GYF domain (residues 529–597; Fig. 1A) in isolation could interact with a TNRC6C PPGL motif peptide (residues 1470–1480, Fig. 1B, blue dashed box). Using the glutathione-S-transferase (GST)-tagged TNRC6C PPGL motif, a direct interaction was detected in pull-down assays with His_6-tagged GIGYF2 GYF domain (Fig. 1C). Similarly, GST-tagged PPGL fragments of TNRC6A and TNRC6B (Fig. 1B) pulled down the His_6-GIGYF2 GYF domain (Fig. 1C). Direct interactions have also been observed between full-length GIGYF2 and TTP from mouse (Fu et al. 2016). We therefore tested whether this interaction was conserved in humans. A GST-tagged fragment of the first tetra-proline region of TTP (residues 68–78, Fig. 1B), which encodes a PPPPGF

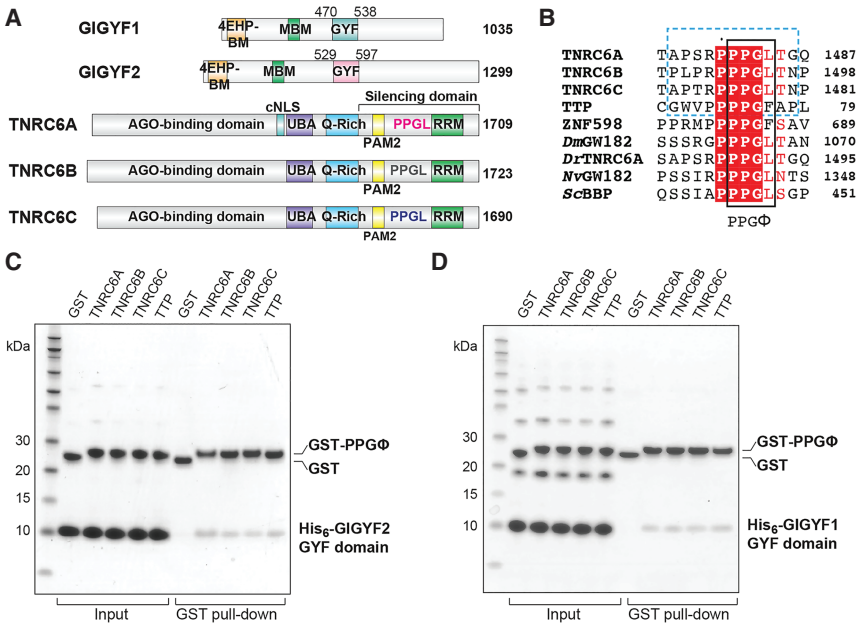

FIGURE 1. GIGYF1/2 GYF domains directly interact with proline-rich sequences from GW182/TNRC6 proteins. (*A*) Schematic representation of human GIGYF1/2 and TNRC6A-C proteins. GIGYF1/2 contain a 4EHP-binding motif (4EHP-BM) and a Me31B/DDX6-binding motif (MBM) within their N-terminal region, as well as a central GYF domain. The conserved PPGL motifs of the TNRC6 proteins are located within their C-terminal silencing domains, which also contains a PAM motif and an RNA-recognition motif (RRM) domain. TNRC6A contains a classical nuclear localization signal (cNLS) between its Argonaute (AGO)-binding domain and ubiquitin-associated motif (UBA). The TNRC6 paralogs also contain Q-rich regions. (*B*) The PPGL motif is conserved in GW182/TNRC6A proteins in metazoa, and proline-rich sequences have been identified in RNA-binding proteins such as TTP and ZNF598. The PPGΦ motif is denoted by the black box, and the peptide sequences used in this study are indicated by the blue dashed box. For comparison, the PRS from *Sc*BBP is also shown. The species abbreviations are as follows: *Dm* (*Drosophila melanogaster*), *Dr* (*Danio rerio*), *Nv* (*Nematostella vectensis*), *Sc* (*Saccharomyces cerevisiae*). (*C*,*D*) GST pull-downs using the recombinant His_6-GIGYF1/2 GYF domain and GST-PRS sequences. GST only served as a negative control.

motif, could also interact with the GIGYF2 GYF domain (Fig. 1C). This analysis is consistent with interactions detected in other studies and extends previous work by refining the minimal molecular requirements of the GIGYF–TNRC6/TTP interactions.

PPGΦ sequences can directly interact with the isolated GIGYF1 GYF domain

Co-immunoprecipitation assays using U2OS cells have detected an interaction between full-length GIGYF1 and TTP (Tollenaere et al. 2019). Deletion of the GYF domain or disruption of the characteristic "GYF" motif in the context of the full-length GIGYF1 protein abolished its interaction with TTP, as well as with ZNF598 which contains three PPPPGF motifs (Tollenaere et al. 2019). Furthermore, a fragment encompassing the GYF domain of GIGYF1 (residues 260–540; Fig. 1A) was sufficient to bind to full-length ZNF598, and mutation of the three ZNF598 PPPPGF motifs could abrogate this interaction in U2OS cells (Tollenaere et al. 2019). As these results indicate that the GYF domain of GIGYF1 might interact with PPGΦ sequences in a similar manner to GIGYF2, we tested whether the isolated GIGYF1 GYF domain could also directly interact with the PPGΦ motifs from the TNRC6 proteins and TTP.

His_6-tagged GIGYF1 GYF domain (residues 470–538; Fig. 1A) interacted with GST-tagged TNRC6 peptides (Fig. 1D). Similar to that observed for GIGYF2, GST-tagged TTP peptide could also directly interact with the GIGYF1 GYF domain (Fig. 1D). Together, this work indicates that the isolated GYF domain of GIGYF1 directly interacts with PPGΦ-containing sequences from binding partners involved in post-transcriptional regulation of gene expression, and that these interactions are conserved between the human GIGYF paralogs.

The GIGYF1/2 GYF domains share structural characteristics typical of the Smy2 subclass of GYF adaptors

While molecular details are available for the CD2BP2 class of GYF domains in humans (Freund et al. 1999, 2002), no structural information is currently available for the human Smy2 class of GYF domains, namely the GYF domains from GIGYF1 and GIGYF2. We therefore determined the crystal structures of the isolated GYF domains from GIGYF2 and GIGYF1 in complex with PPGL peptides from TNRC6A and TNRC6C, respectively (Fig. 2A,B; Supplemental Table S1). Crystals of the TNRC6C–GIGYF1 GYF domain complex were obtained in the C121 space group and diffracted to 1.79 Å resolution. The asymmetric unit comprises two TNRC6C–GIGYF1 complexes that display high similarity (root mean square deviation [RMSD] of 0.4 Å over 61 Cα atoms). The TNRC6A–GIGYF2 GYF domain complex crystallized in the $P2_12_12_1$ space group with one heterodimer in the asymmetric unit, and the structure was refined to 1.23 Å resolution.

The GYF domains of GIGYF1 and GIGYF2 are comprised of a four-stranded antiparallel β-sheet with two α-helices that pack onto one face (Fig. 2A,B). The structures of the GYF domains from the human GIGYF proteins are highly conserved (Fig. 2C) with a backbone RMSD of 1.2 Å over 60 Cα atoms. The human GIGYF structures also display a high degree of structural similarity with *Sc*Smy2

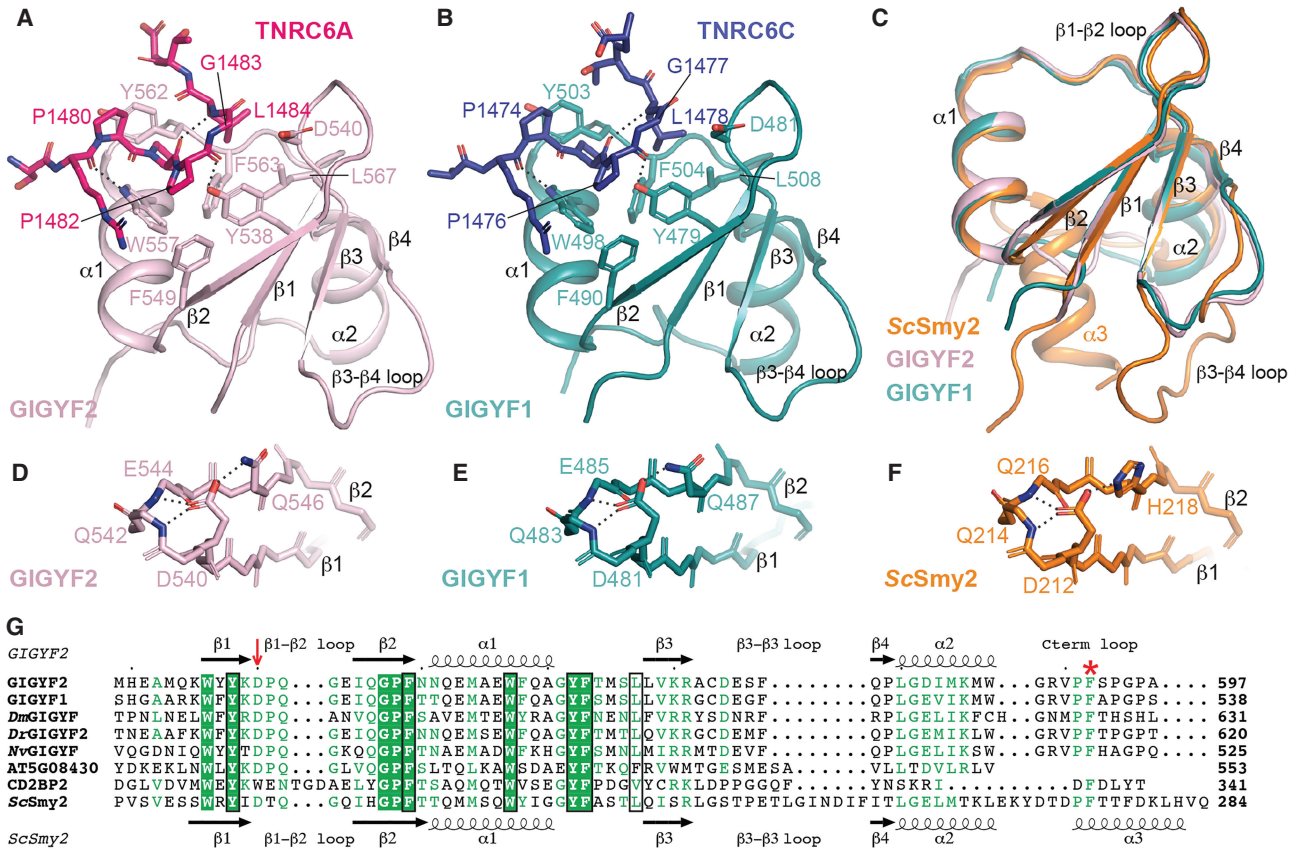

FIGURE 2. Overall structures of GIGYF1/2 GYF domains in complex with TNRC6 PPGL-containing peptides. (*A*) The TNRC6A PRS peptide (hot pink sticks) binds to a conserved arrangement of aromatic residues on the surface of the GIGYF2 GYF domain (light pink cartoon). Hydrogen bonds are denoted by dashed lines. Similar interactions are observed between the TNRC6C PRS peptide (navy sticks) and the GIGYF1 GYF domain (teal cartoon) (*B*). (*C*) The GIGYF1/2 GYF domains are highly similar to the *Sc*Smy2 GYF fold (orange; PDB ID 3FMA [Ash et al. 2010]). (*D–F*) The conserved Asp residue that defines the Smy2 class of GYF domains mediates analogous interactions in GIGYF1/2 and *Sc*Smy2. (*G*) Structural-based sequence alignment of GYF domains. The prototypical Asp residue of the Smy2 GYF subclass is indicated by the red arrow. The residues that comprise the PRS-binding surface are boxed in black. The Phe plug is denoted by the red asterisk.

GYF domain with RMSD values of 1.1 and 1.3 Å for GIGYF1 and GIGYF2, respectively (over 56 and 59 Cα positions). The secondary structures superimpose well, though there are some deviations in the β3–β4 loop, as well as the C terminus of the domains whereby *Sc*Smy2 contains an additional α3 helix (Fig. 2C).

One of the defining features of the Smy2-subclass of GYF domains is a conserved Asp residue (D540 in GIGYF2, D481 in GIGYF1, and D212 in *Sc*Smy2, denoted by red arrow in Fig. 2G) within the β1–β2 loop (Kofler and Freund 2006; Ash et al. 2010). In our structures, GIGYF2 D540 and GIGYF1 D481 interact with a hydrogen bond donor present on the β2 strand (Q546 in GIGYF2, and Q487 in GIGYF1), which is analogous to H218 in *Sc*Smy2 (Fig. 2D–F). The orientation of D540 and D481 in the human GIGYF proteins is further stabilized by hydrogen bonds with the backbone amides of the β1–β2 loop (Q483 and E485 in GIGYF1, and Q542 and E544 in GIGYF2; Fig. 2D,E). Identical interactions are observed for D212 in the *Sc*Smy2 structure (Fig. 2F). Our structures reveal that the overall architecture of the Smy2 subfamily of GYF domains is conserved between yeast and humans.

The GIGYF1 and GIGYF2 GYF domains interact with PPGL sequences

The crystals of human GIGYF GYF domains were obtained in complex with PPGL peptides from TNRC6A and TNRC6C, and the peptides could be built unambiguously into strong density located at the canonical PRS-binding surface (Fig. 2A,B; Supplemental Fig. S1A,B). A series of residues in the GYF domains form a hydrophobic PRS-binding groove (Fig. 3A,B). These residues are Y538, F549, W557, Y562, F563, L567 in GIGYF2, and Y479, F490, W498, Y503, F504, L508 in GIGYF1 (Fig. 3A,B). Two hydrogen bonds are formed between GIGYF2 residues Y538 and W557 and the TNRC6A peptide backbone (Figs. 2A, 3A). Analogous interactions are observed in the GIGYF1–TNRC6C, *Sc*Smy2–BBP and CD2BP2–CD2

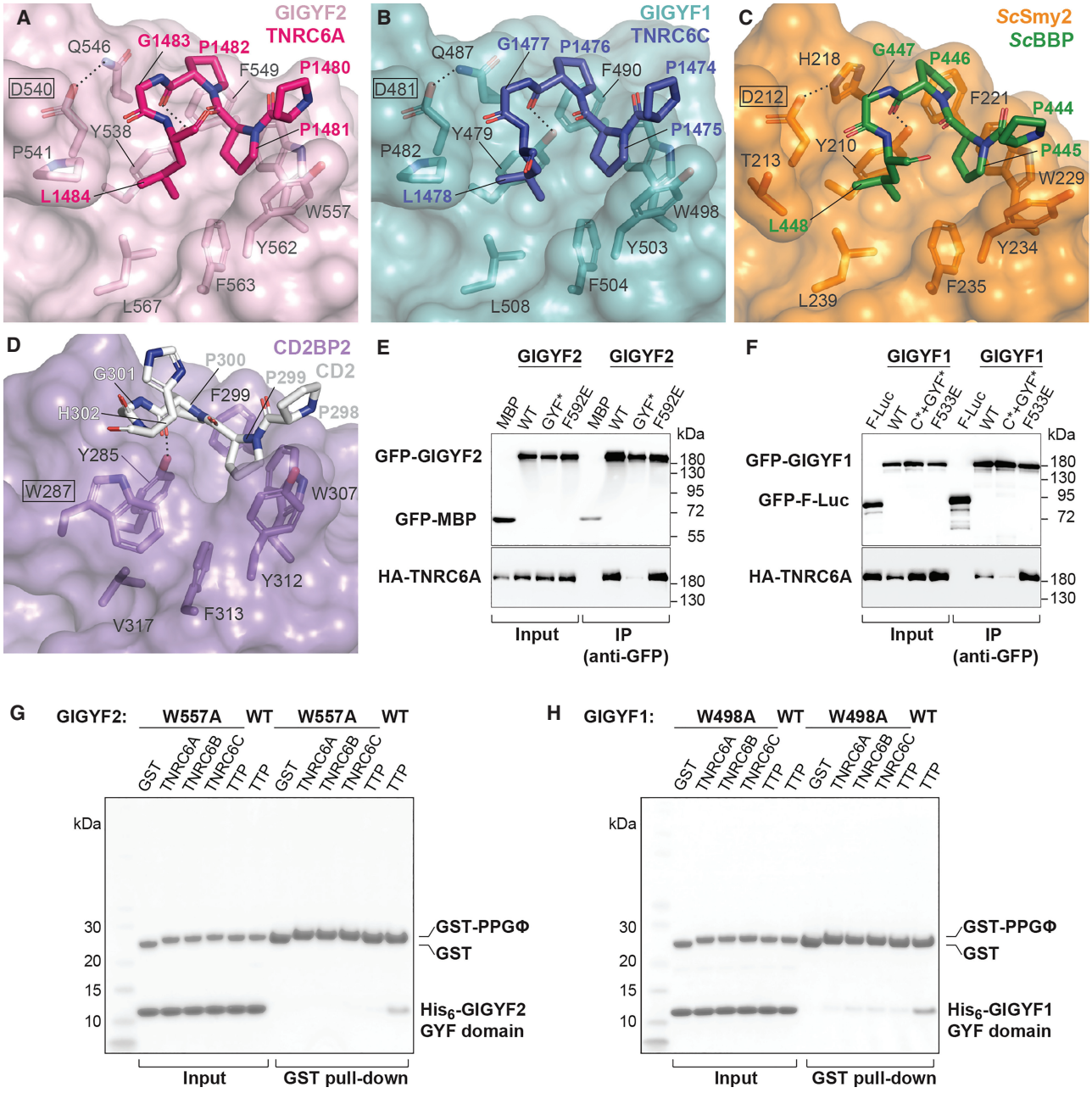

FIGURE 3. Proline-rich sequences bind to a conserved hydrophobic depression on the GYF domain surface. (*A–C*) Close-up views of TNRC6A, TNRC6C, and *Sc*BBP peptides binding to the GYF domains of GIGYF2, GIGYF1, and *Sc*Smy2 (PDB ID 3FMA), respectively. The defining Asp residue of the Smy2 class of GYF domains are indicated by black boxes. In contrast, the CD2BP2 class of GYF domains contain a Trp (W287 in human CD2BP2, boxed; PDB ID 1L2Z [Freund et al. 2002]) at this position (*D*). The conserved Trp in CD2BP2 GYF domains disrupt the hydrophobic cavity, which is exploited by PRS-containing sequences in the Smy2 class of GYF domains. (*E*,*F*) GFP-tagged full-length GIGYF1/2 interacts with HA-tagged full-length TNRC6A in HEK293T cells, and substitution of four residues within the PPGΦ-binding site (GYF*) disrupted this interaction, as indicated by western blot analysis. The interaction was not affected by Phe plug mutations F592E and F533E in GIGYF2 and GIGYF1, respectively. GFP-MBP and GFP-F-Luc served as negative controls. (*G*,*H*) Pull-down assays using purified His_6-GIGYF1/2 GYF domain and GST-PRS sequences. A single mutation within the PPGΦ-binding site of GIGYF2 and GIGYF1 (W557A and W498A, respectively) reduced the interactions in vitro.

complex structures (Figs. 2B, 3B–D; Freund et al. 2002; Ash et al. 2010). Mutation of four of the PRS-binding groove residues in full length GIGYF1 and GIGYF2 (GYF*, Supplemental Table S2), including the characteristic "GYF" motif, severely compromised the ability of the proteins to interact with TNRC6A in cells (Fig. 3E,F). This is consistent with previous work demonstrating that a single substitution within the prototypic "GYF" motif could

abrogate the interaction between GIGYF1 and ZNF598 (Tollenaere et al. 2019).

The TNRC6A PPGΦ motif adopts a polyproline II (PPII) helix with P1481 and P1482 interacting with the hydrophobic surface comprised of GIGYF2 Y538, F549, W557, and Y562. In this conformation, P1481 stacks against W557 in an aromatic pocket formed by F549 and Y562 (Fig. 3A). The TNRC6C PPGΦ motif similarly forms a PPII helical conformation, with P1475 stacking against W498 of GIGYF1 (Fig. 3B). Mutation of W557 and W498 to Ala in the isolated GYF domains of GIGYF2 and GIGYF1, respectively, markedly decreased association with GST-tagged TNRC6 and TTP peptides in vitro (Fig. 3G,H). The requirement for the Gly residue within the PPGΦ consensus is structurally rationalized as any larger side chain would clash with the conserved D540 and Q546 of the GIGYF2 GYF domain (or D481 and Q487 in GIGYF1, respectively; Fig. 3A,B; Ash et al. 2010).

The Gly residue within the PPGΦ motif facilitates the adoption of turn in trajectory, enabling the subsequent hydrophobic residue (Φ) to insert into a hydrophobic cavity lined by Y538, F563, and L567 of GIGYF2 (Y479, F504, and L508 in GIGYF1). This cavity is surface-exposed owing to the conformation of the characteristic Smy2-subclass Asp residue that orients away from this surface in GIGYF2, GIGYF1, and *Sc*Smy2 (boxed in Fig. 3A–C). In contrast, the CD2BP2 subfamily of GYF domains contain a Trp in place of the Asp in the β1–β2 loop (Fig. 2G red arrow; boxed in Fig. 3D), which acts as a cover to obscure the hydrophobic surface formed by Y285, V317, and F313 (Fig. 3D; Freund et al. 2002; Kofler and Freund 2006; Ash et al. 2010). The different surfaces created by the defining Asp and Trp residues in the Smy2 and CD2BP2 subfamilies, respectively, thereby determine the PRS-binding specificities of the GYF domains by either extending or discontinuing the hydrophobic PRS-binding surface (Ash et al. 2010).

TNRC6A and TNRC6C both contain Leu residues within their PPGΦ motifs, which are inserted into the Smy2 subclass-specific cavity of the GIGYF GYF domains. The TNRC6 peptides bind to the GYF adaptors in a manner highly similar to that observed when *Sc*BBP interacts with *Sc*Smy2 (Fig. 3C; Ash et al. 2010). Our structures, together with the *Sc*Smy2–*Sc*BBP complex structure (Ash et al. 2010), reveal that the Smy2 subclass-specific cavity can accommodate larger hydrophobic sidechains, such as the Phe observed in the TTP and ZNF598 PPGΦ motifs (Fig. 1B). However, the cavity is too small to fit the Trp indole moiety without rearrangements within the binding pocket, consistent with the consensus identified by phage display analyses (Kofler et al. 2005).

The "RPPPGL" sequence shared between TNRC6A and TNRC6C adopt similar conformations in our structures (Fig. 2A,B). It is therefore highly likely that TNRC6A interacts with GIGYF1 in a similar manner to that observed for TNRC6C, and, likewise, that TNRC6C interacts in an analogous manner to TNRC6A when binding to GIGYF2, corroborated by the similar binding properties seen in our pulldown studies (Fig. 1C,D). The "RPPPGL" motif is also present in TNRC6B (Fig. 1B; Mishima et al. 2012), and given the high similarity between the GIGYF2–TNRC6A and GIGYF1–TNRC6C structures, we would expect that comparable interactions would be mediated between TNRC6B and the GIGYF1/2 GYF domains. More broadly, the residues that comprise the GIGYF PRS-binding site, and the TNRC6/GW182 "PPGL" motif, are highly conserved from cnidaria (*Nematostella vectensis*; *Nv*) to humans (Figs. 1B, 2G; Moran et al. 2013). While sequence conservation suggests that the structures determined here would be suitable models of GIGYF–GW182 interactions in different species, we have previously shown that *Drosophila melanogaster* (*Dm*) GW182 did not bind to *Dm*GIGYF under the conditions tested (Ruscica et al. 2019). The binding partners of GIGYF proteins do not appear to be strictly conserved between *Dm* and humans with *Dm*GIGYF failing to associate with the PRS-containing *Dm*ZNF598. While the molecular basis of differential binding in *Dm* and humans is still unclear, comparison of AlphaFold models (Jumper et al. 2021) of the full-length *Dm*GW182 and human TNRC6 proteins suggests that the PPGL motif may be more accessible in the human proteins compared with *Dm*GW182 (Supplemental Fig. S1C–F).

A conserved C-terminal Phe side chain is inserted into a hydrophobic pocket in GYF domains from yeast to humans

The N-terminal half of the GYF domains, comprising β1, β2, α1, and α1–β3 loop structural elements, are responsible for ligand binding and are highly conserved between GYF domain family members (Kofler and Freund 2006). In contrast, the C-terminal regions of GYF domains are poorly conserved, differing in length and composition (Kofler and Freund 2006). This is exemplified by *Sc*Smy2 which contains a C-terminal α3 helix (Ash et al. 2010) not present in the human GIGYF1/2 GYF domains (Fig. 2A–C,G). Due to the sequence identity between the GIGYF1 and GIGYF2 GYF domains (~80% identical), even the C-terminal portions are highly similar with only slight differences observed in the conformations β3–β4 loop, and the C-terminal loop of the GYF domains (Fig. 4A).

Although there are slight differences in the C-terminal loop between the human GIGYF domain structures, the position of a Phe side chain adopts highly similar positions in GIGYF1 and GIGYF2 (F533 and F592, respectively; Fig. 4A denoted by red asterisk). Superimposition of the human GIGYF structures with *Sc*Smy2 reveals an analogous Phe side chain at this position encoded at the start of the α3 helix (Fig. 4B, red asterisk), despite the conformational

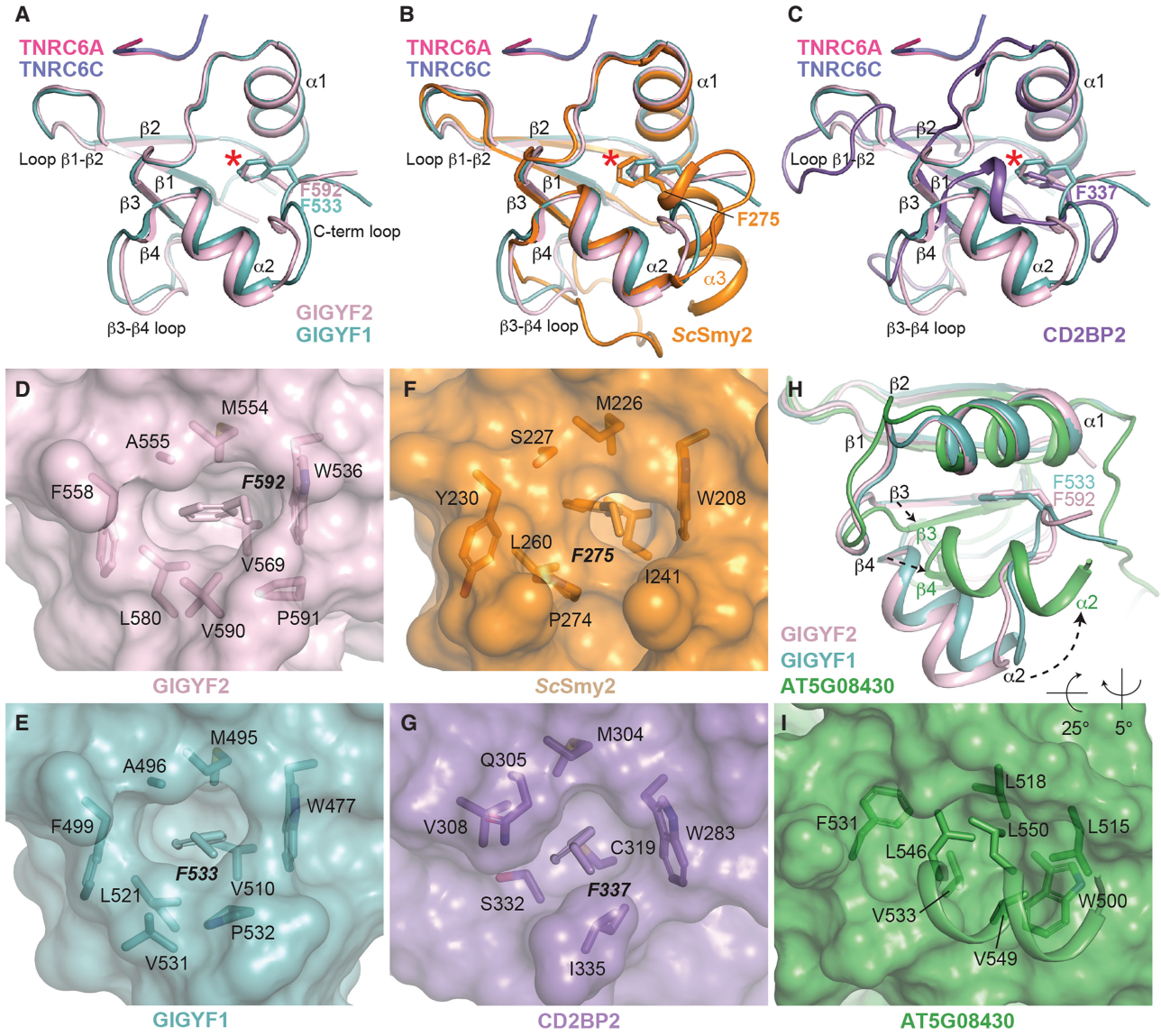

FIGURE 4. A conserved Phe residue is found at the C terminus of Smy2 and CD2BP2 GYF domain classes from yeast to humans. (*A*) Superimposition of GYF domains from GIGYF1 and GIGYF2, shown in teal and light pink, respectively. The TNRC6 peptides are shown in hot pink and navy cartoon representation. The conserved Phe residue is shown in sticks and indicated by a red asterisk. The same view is shown in *B* and *C*, but with *Sc*Smy2 (orange; PDB ID 3FMA) and CD2BP2 (purple; PDB ID 1L2Z) superimposed, respectively. (*D*–*G*) Surface representation of GIGYF2, GIGYF1, *Sc*Smy2 (PDB ID 3FMA), and CD2BP2 (PDB ID 1L2Z), respectively, with residues surrounding the Phe plug shown in sticks. (*H*) Superimposition of GIGYF2 and GIGYF1 with *A. thaliana* ATG08430 (green; PDB ID 1WH2). The GYF domain of *A. thaliana* ATG08430 is found at the extreme C-terminal end of the protein and does not encode a Phe plug residue. Conformational changes are observed between the *A. thaliana* ATG08430 and GIGYF1/2 in the α2 helix, as well as the β3 and β4 strands of the GYF domain. (*I*) The α2 helix in the plant GYF domain packs against the hydrophobic surface in the absence of a Phe plug.

variability observed between yeast and human proteins in this region. The structure of the *Sc*Smy2 GYF domain has previously been determined in a domain-swapped arrangement (PDB IDs 3K3V and 3FMA) with C-terminal α3 helices interacting with an adjacent GYF domain. Interestingly, the interactions between the F275 side chain are maintained in the domain-swapped conformation, which is inserted into the hydrophobic pocket of a neighboring GYF domain (Ash et al. 2010). Moreover, a phenyl moiety is also observed in a similar orientation in the CD2BP2 GYF domain notwithstanding the large differences observed between the C-terminal regions of CD2BP2 and the Smy2-classes of GYF domains (Fig. 4C, red asterisk).

Close inspection of the C-terminal Phe residues in GIGYF1/2, *Sc*Smy2, and CD2BP2 (F592, F533, F275, and F337 in GIGYF2, GIGYF1, *Sc*Smy2, and CD2BP2, respectively) reveals that the Phe side chain is inserted, like a

plug, into a hydrophobic cavity that is formed between the α1 and α2 helices and the inside face of the β-sheet (Fig. 4D–G). In this position, the conserved C-terminal Phe, which we term the "Phe plug," forms part of the hydrophobic core of the small adaptor domains. Examination of GIGYF and CD2BP2 sequences from yeast to humans reveals strict conservation of this C-terminal Phe plug residue in both GIGYF and CD2BP2 GYF domain sequences (Fig. 2G; Supplemental Fig. S2 denoted by a red asterisk). While this feature is not annotated as part of the GYF domain in some online databases, the general position of the Phe plug was predicted by AlphaFold (Supplemental Fig. S3A,B; Jumper et al. 2021).

The Phe plug is not conserved in Arabidopsis GYF domains

In contrast, the Phe plug is absent in the only plant GYF domain whose structure has been determined (from gene AT5G08430; Fig. 4H, PDB code 1WH2). The *Arabidopsis thaliana* AT5G08430 GYF domain is more divergent from the human GIGYF structures than *Sc*Smy2 and CD2BP2 with larger RMSD values (2.4 and 2.3 Å for GIGYF1 and GIGYF2, respectively) and lower DALI server *Z*-scores (*Z*-scores above 6.2 for CD2BP2 and *Sc*Smy2, and lower than 5.8 for AT5G08430).

The AT5G08430 GYF domain is located at the extreme C-terminal end of the protein with no additional residues encoded after the α2 helix (Fig. 2G; Supplemental Fig. S3C). Compared with the α2 helix of GIGYF GYF domains, the AT5G08430 α2 helix is positioned closer to the α1 helix. In this orientation, hydrophobic side chains L546, V549, and L550 from the AT5G08430 α2 helix pack against the hydrophobic surface formed by W500, L515, and L518 (Fig. 4H,I). *A. thaliana* encodes several GYF domain-containing proteins, and structural prediction by AlphaFold suggests that these domains have a similar fold to AT5G08430 with RMSD values between 0.7–1.9 Å (Supplemental Fig. S3C,D). While three SWIB/PHD/GYF domain-containing proteins contain a Phe residue directly C-terminal to the α2 helix (AT2G18090, AT2G16485/NERD, AT3G51120; highlighted by a dashed red box in Supplemental Fig. S3C,E), the predicted conformation of these Phe side chains is dissimilar to that observed for the GIGYF2 Phe plug. Other *A. thaliana* GYF domain-containing proteins (AT5G42950/EXA1, AT1G24300, and AT1G27430) do not encode obvious Phe plug residues at the C terminus of their GYF domains (Supplemental Fig. S3C,F). Notably, the GIGYF ortholog in *A. thaliana*, AT5G42950/EXA1, encodes a PPPGF sequence in this region that is thought to act as an autoinhibitory sequence to prevent low affinity interactions with the GYF domain (boxed blue in Supplemental Fig. S3C; Kofler and Freund 2006). Together, our structural analysis has revealed the presence of a conserved Phe plug at the C terminus of CD2BP2 and GIGYF classes of GYF domains from yeast to humans. Sequence analyses, however, indicate that this feature may not be present in *A. thaliana* GYF domains.

The Phe plug contributes to GIGYF2 GYF domain stability

To investigate the importance of the conserved C-terminal Phe plug, we generated GYF domain mutants that disrupted the hydrophobic nature of the plug. More specifically, we replaced the Phe plug with the negatively charged Glu residue generating GIGYF1 F533E and GIGYF2 F592E mutants. The His_6-tagged mutant GYF domains were then tested for their ability to bind to the PRS sequences of TNRC6A and TTP. As the Phe residue is distal to the PRS binding site, the substitution did not affect the binding of PRS-containing sequences in GST pull-down assays under the conditions tested (Supplemental Fig. S4A, B). Co-immunoprecipitation analysis also suggested that the F533E and F592E mutations in GIGYF1 and GIGYF2, respectively, did not affect binding to TNRC6A or 4EHP in cells (Fig. 3E,F; Supplemental Fig. S4C,D). Thermal stability assays, however, indicated that mutation of the Phe plug decreased the stability of the isolated GIGYF2 GYF domain with the apparent melting temperature of the F592E mutant 7°C lower than that observed for the wild-type domain (Tm_{app} of 60°C and 53°C for the wild-type and F533E GYF domains, respectively; Supplemental Fig. S4E). In contrast, the more conservative substitution F592W displayed very similar binding and thermal stability properties as the wild-type GIGYF2 GYF domain (Supplemental Fig. S4E,G). Similar in vitro binding results were obtained for the analogous F533W mutation in the GIGYF1 GYF domain (Supplemental Fig. S4F). Our analyses suggest that the hydrophobic and aromatic Phe plug contributes to the stability of the GIGYF2 GYF domain, but the integrity of the Phe plug residue is not strictly required for PRS binding in vitro and in cells. This is consistent with the observation that the Phe plug is not present in the *A. thaliana* AT5G08430 GYF, although it is currently unclear if this domain can bind to PRS-containing proteins in plants. These results therefore refine our understanding of the molecular features of GYF domain adaptors, which should be taken into consideration when designing GYF domain constructs.

In this study, we have elucidated the molecular basis of TNRC6 recognition by human GIGYF1/2 GYF domains. Previous work has indicated that GIGYF2 may regulate miRISC activity (Schopp et al. 2017), and our work reveals the molecular basis of 4EHP-mediated translational repression of miRNA targets via the GIGYF1/2–TNRC6 interaction. While this study focuses on the TNRC6 proteins and TTP, other PRS-containing factors involved in translational regulation are known to interact with the GIGYF

proteins in eukaryotic cells (Ash et al. 2010; Morita et al. 2012; Amaya Ramirez et al. 2018; Ruscica et al. 2019; Tollenaere et al. 2019; Mayya et al. 2021). As such, the molecular details we outline here are likely to be conserved in a variety of biological contexts to elicit 4EHP-mediated repression. Mutations in *GIGYF2* have been implicated in neurological conditions such as autism spectrum disorder and schizophrenia (Iossifov et al. 2014; Krumm et al. 2015; Thyme et al. 2019; Satterstrom et al. 2020). Although the role of *GIGYF2* mutants in the aetiology of these neurological conditions is still unclear, recent work has revealed the importance of the GIGYF2–4EHP axis in protein quality control (Hickey et al. 2020; Juszkiewicz et al. 2020; Sinha et al. 2020; Weber et al. 2020). It is therefore tempting to speculate that the impairment of GIGYF2 function may lead to the accumulation of misfolded and potentially cytotoxic polypeptide products that contribute to the development of neurological conditions.

MATERIALS AND METHODS

DNA constructs

DNA constructs used in this study are listed in Supplemental Table S2. Mutants used in this study were generated by site-directed mutagenesis using the QuickChange Site-Directed Mutagenesis kit (Stratagene). All constructs were confirmed by sequencing.

Protein expression and purification

GST-PPGL and GST-TTP fragments were expressed in BL21(DE3) cells overnight at 18°C. The GST-fusion proteins were purified in 50 mM Tris 7.5, 125 mM NaCl, 2 mM 2-mercaptoethanol (BME). The His_6-GIGYF2 GYF domain was expressed in BL21(DE3) cells at 20°C overnight, and pellets were resuspended in 50 mM Tris 8.0, 400 mM NaCl, 2 mM imidazole, 5 mM BME. The His_6-GIGYF2 GYF domain was eluted from a Ni-NTA column (GE Healthcare) using 250 mM imidazole and further purified using a S200 10/600 column (GE Healthcare) and flash frozen in 10 mM Tris 8.0, 150 mM NaCl, 5 mM BME. His_6-GIGYF1 GYF domain was expressed and purified in similar conditions to GIGYF2. His_6-GIGYF1/2 mutants were expressed and purified using similar conditions as the wild-type domains. Both wild-type and F533E/F533W mutant GIGYF1 GYF domains appeared to be less stable than the isolated GIGYF2 GYF domains. We were unable to purify GYF domain mutants containing four (GYF*, Supplemental Table S2) and six Ala substitutions within the PRS-binding site. GIGYF2–TNRC6A complexes were obtained by immobilizing GST-TNRC6A PPGL fragments on a GSTrap column and binding to purified GIGYF2 protein. The complex was eluted using 10 mM glutathione, and the GST tag was cleaved overnight using GST-3C protease. The complex was purified from GST using size exclusion chromatography. GIGYF1–TNRC6C complexes were purified using similar conditions.

Crystallization and data collection

Crystals of GIGYF2 GYF domain (residues 529–597) in complex with TNRC6A PPGL motif (residues 1476–1486) were obtained in 1.0–1.4 M Na/K phosphate pH 7.4–7.8 and were flash frozen in liquid nitrogen using 25% glycerol as a cryoprotectant. Crystals of GIGYF1 GYF domain (residues 470–538) in complex with TNRC6C PPGL motif (1470–1480) were obtained in 100 mM Hepes 7.0, 1 M sodium malonate, and 25% glycerol was used as a cryoprotectant before freezing. Data were collected at the Australian Synchrotron MX2 beamline (McPhillips et al. 2002; Aragão et al. 2018) and processed using XDS (Kabsch 2010). For the GIGYF2–TNRC6A complex, *Sc*Smy2 was used as a molecular replacement model with *Sc*BBP coordinates removed (PDB ID 3FMA) (Ash et al. 2010). For the GIGYF1–TNRC6C, the GIGYF2 structure was used as the search model (TNRC6A coordinates removed) in PHASER (McCoy et al. 2007). Refinement was performed in Phenix (Liebschner et al. 2019), and both structures have excellent geometry (Supplemental Table S1; Williams et al. 2018).

GST pull-down

Pull-down assays were performed essentially as described previously. Specifically, 80 µg of GST or GST-PPGL/GST-TTP fragments were incubated with 160 µg of His_6-GIGYF2 or His_6-GIGYF1 GYF domains in the presence of 25 µL of glutathione superflow agarose (Pierce) preequilibrated in binding buffer (50 mM Tris 7.5, 125 mM NaCl, 2 mM BME). The resin was washed four times in binding buffer, and bound proteins were eluted with binding buffer supplemented with 20 mM glutathione. The samples were analyzed using SDS-PAGE, input lanes correspond to 2% of incubated protein and pull-down lanes correspond to 10% of eluted sample.

Thermal shift assays

Purified His_6-GIGYF2 GYF domain, wild-type and F592E/F592W mutants in 10 mM Tris 7.5, 150 mM NaCl, 5mM BME were mixed with SYPRO orange (Sigma; 5× final concentration) and dispensed into a 96-well qPCR plate. The solution was slowly heated from 4°C to 95°C using an Applied Biosystems StepOnePlus real-time qPCR machine. Fluorescence was detected using a ROX filter. The data were analyzed using the StepOne Software and the minimum of the negative first derivative was used to determine the apparent melting temperature (Tm_{app}). Assays were performed in triplicate. Similar calculations could not be performed with the isolated wild-type GIGYF1 GYF domain and the F592E/F592W mutants which displayed high initial fluorescence and ambiguous melt transition, consistent with the instability of the domains observed during purification. Lysozyme was used as a positive control and the apparent melting temperature is similar to previous reports (Deore and Manderville 2019).

Co-immunoprecipitation (Co-IP) assays

Co-IP assays were performed as described previously (Peter et al. 2015). HEK293T cells were grown in 10 cm dishes and transfected using Lipofectamine 2000 (Invitrogen) according to the

manufacturer's recommendations. The transfection mixtures contained 8 µg of GFP-MBP, 8 µg of GFP-F-LUC, 6.5 µg GFP-GIGYF1, 7 µg of GFP-GIGYF1 C*, 7 µg of GFP-GIGYF1 C* GYF*, 7 µg of GFP-GIGYF1 F533E, 8 µg of GFP-GIGYF2, 7 µg of GFP-GIGYF2 C*, 10 µg of GFP-GIGYF2 GYF*, or 10 µg of GFP-GIGYF2 F592E. Cells were harvested 48 h post transfection, washed with ice cold PBS and lysed on ice for 15 min in 500 µL of NET buffer [50 mM Tris-HCl 7.5, 150 mM NaCl, 0.1% Triton X-100, 1 mM EDTA 8.0, 10% glycerol, supplemented with 1x protease inhibitors (Roche)]. Cell debris was removed by centrifugation at 16,000*g* at 4°C. Input samples were collected for western blotting. To immunoprecipitate GFP-tagged proteins, the remaining lysate was then incubated with 3 µL of anti-GFP antibody (homemade) for an hour, followed by incubation (2 h) with protein G sepharose resin (50% slurry). Beads were washed three times with NET buffer and resuspended in 1 mL of NET buffer without detergent. The bead suspension was mixed with SDS-PAGE sample buffer for western blotting after centrifugation to pellet the resin. Input lanes correspond to 0.5% of the total cell lysate and immunoprecipitation lanes correspond to 5% and 10% of the GFP and HA proteins, respectively.

Western blotting

Western blot was performed using standard methods. In brief, cells were washed with PBS and lysed with sample buffer (100 mM Tris-HCl 6.8, 4% SDS, 20% glycerol, 0.2 M DTT) followed by boiling 5 min at 95°C and vortexing to shear genomic DNA. After SDS-PAGE, proteins were transferred onto a nitrocellulose membrane (Santa Cruz Biotechnology) by tank transfer. Primary antibodies were incubated overnight at 4°C, secondary antibodies for an hour at room temperature. All western blots were developed with Clarity Western ECL substrate solutions (Bio-Rad). Antibodies were as follows: Rabbit polyclonal anti-GFP (in house; 1:2000), Mouse monoclonal anti-HA (HRP) (Roche; 1:5000), Donkey polyclonal anti-rabbit IgG (HRP) (GE Healthcare).

DATA DEPOSITION

The coordinates of GIGYF1–TNRC6C (7RUQ) and GIGYF2–TNRC6A (7RUP) have been deposited into the Protein Data Bank.

SUPPLEMENTAL MATERIAL

Supplemental material is available for this article.

ACKNOWLEDGMENTS

We thank the beamline scientists at the Australian Synchrotron for their assistance with data collection. This research was undertaken in part using the MX2 beamline at the Australian Synchrotron, part of ANSTO, and made use of the Australian Cancer Research Foundation (ACRF) detector. A.G.S. was supported by a National Health and Medical Research Council Fellowship APP1159347 and grant APP1146403. M.C. was supported by Australian Research Council Fellowship DE160100608 and Australian Research Council grant DP220102497. C.I. was supported by the Max Planck Society.

Received January 13, 2023; accepted February 5, 2023.

REFERENCES

Amaya Ramirez CC, Hubbe P, Mandel N, Béthune J. 2018. 4EHP-independent repression of endogenous mRNAs by the RNA-binding protein GIGYF2. *Nucleic Acids Res* **46:** 5792–5808. doi:10.1093/nar/gky198

Aragão D, Aishima J, Cherukuvada H, Clarken R, Clift M, Cowieson NP, Ericsson DJ, Gee CL, Macedo S, Mudie N, et al. 2018. MX2: a high-flux undulator microfocus beamline serving both the chemical and macromolecular crystallography communities at the Australian Synchrotron. *J Synchrotron Radiat* **25:** 885–891. doi:10.1107/S1600577518003120

Ash M-R, Faelber K, Kosslick D, Albert GI, Roske Y, Kofler M, Schuemann M, Krause E, Freund C. 2010. Conserved β-hairpin recognition by the GYF domains of Smy2 and GIGYF2 in mRNA surveillance and vesicular transport complexes. *Structure* **18:** 944–954. doi:10.1016/j.str.2010.04.020

Chapat C, Jafarnejad SM, Matta-Camacho E, Hesketh GG, Gelbart IA, Attig J, Gkogkas CG, Alain T, Stern-Ginossar N, Fabian MR, et al. 2017. Cap-binding protein 4EHP effects translation silencing by microRNAs. *Proc Natl Acad Sci* **114:** 5425. doi:10.1073/pnas.1701488114

Deore PS, Manderville RA. 2019. Aptamer-induced thermofluorimetric protein stabilization and G-quadruplex nucleic acid staining by SYPRO orange dye. *New Journal Chem* **43:** 4994–4997. doi:10.1039/C9NJ00188C

Freund C, Dötsch V, Nishizawa K, Reinherz EL, Wagner G. 1999. The GYF domain is a novel structural fold that is involved in lymphoid signaling through proline-rich sequences. *Nat Struct Biol* **6:** 656–660. doi:10.1038/10712

Freund C, Kühne R, Yang H, Park S, Reinherz EL, Wagner G. 2002. Dynamic interaction of CD2 with the GYF and the SH3 domain of compartmentalized effector molecules. *EMBO J* **21:** 5985–5995. doi:10.1093/emboj/cdf602

Fu R, Olsen MT, Webb K, Bennett EJ, Lykke-Andersen J. 2016. Recruitment of the 4EHP-GYF2 cap-binding complex to tetraproline motifs of tristetraprolin promotes repression and degradation of mRNAs with AU-rich elements. *RNA* **22:** 373–382. doi:10.1261/rna.054833.115

Giovannone B, Tsiaras WG, de la Monte S, Klysik J, Lautier C, Karashchuk G, Goldwurm S, Smith RJ. 2009. GIGYF2 gene disruption in mice results in neurodegeneration and altered insulin-like growth factor signaling. *Hum Mol Genet* **18:** 4629–4639. doi:10.1093/hmg/ddp430

Hernández G, Altmann M, Sierra JM, Urlaub H, Diez del Corral R, Schwartz P, Rivera-Pomar R. 2005. Functional analysis of seven genes encoding eight translation initiation factor 4E (eIF4E) isoforms in *Drosophila*. *Mech Dev* **122:** 529–543. doi:10.1016/j.mod.2004.11.011

Hickey KL, Dickson K, Cogan JZ, Replogle JM, Schoof M, D'Orazio KN, Sinha NK, Hussmann JA, Jost M, Frost A, et al. 2020. GIGYF2 and 4EHP inhibit translation initiation of defective messenger RNAs to assist ribosome-associated quality control. *Mol Cell* **79:** 950–962.e956. doi:10.1016/j.molcel.2020.07.007

Iossifov I, O'Roak BJ, Sanders SJ, Ronemus M, Krumm N, Levy D, Stessman HA, Witherspoon KT, Vives L, Patterson KE, et al. 2014. The contribution of de novo coding mutations to autism spectrum disorder. *Nature* **515:** 216–221. doi:10.1038/nature13908

Jackson RJ, Hellen CUT, Pestova TV. 2010. The mechanism of eukaryotic translation initiation and principles of its regulation. *Nat Rev Mol Cell Biol* **11:** 113–127. doi:10.1038/nrm2838

Jonas S, Izaurralde E. 2015. Towards a molecular understanding of microRNA-mediated gene silencing. *Nat Rev Genet* **16:** 421–433. doi:10.1038/nrg3965

Joshi B, Cameron A, Jagus R. 2004. Characterization of mammalian eIF4E-family members. *Eur J Biochem* **271:** 2189–2203. doi:10.1111/j.1432-1033.2004.04149.x

Jumper J, Evans R, Pritzel A, Green T, Figurnov M, Ronneberger O, Tunyasuvunakool K, Bates R, Žídek A, Potapenko A, et al. 2021. Highly accurate protein structure prediction with AlphaFold. *Nature* **596:** 583–589. doi:10.1038/s41586-021-03819-2

Juszkiewicz S, Slodkowicz G, Lin Z, Freire-Pritchett P, Peak-Chew S-Y, Hegde RS. 2020. Ribosome collisions trigger *cis*-acting feedback inhibition of translation initiation. *Elife* **9:** e60038. doi:10.7554/eLife.60038

Kabsch W. 2010. XDS. *Acta Crystallogr D Biol Crystallogr* **66:** 125–132. doi:10.1107/S0907444909047337

Kofler MM, Freund C. 2006. The GYF domain. *FEBS J* **273:** 245–256. doi:10.1111/j.1742-4658.2005.05078.x

Kofler M, Motzny K, Freund C. 2005. GYF domain proteomics reveals interaction sites in known and novel target proteins. *Mol Cell. Proteomics* **4:** 1797–1811. doi:10.1074/mcp.M500129-MCP200

Krumm N, Turner TN, Baker C, Vives L, Mohajeri K, Witherspoon K, Raja A, Coe BP, Stessman HA, He Z-X, et al. 2015. Excess of rare, inherited truncating mutations in autism. *Nat Genet* **47:** 582–588. doi:10.1038/ng.3303

Liebschner D, Afonine PV, Baker ML, Bunkoczi G, Chen VB, Croll TI, Hintze B, Hung L-W, Jain S, McCoy AJ, et al. 2019. Macromolecular structure determination using X-rays, neutrons and electrons: recent developments in Phenix. *Acta Crystallogr D Struct Biol* **75:** 861–877. doi:10.1107/S2059798319011471

Mader S, Lee H, Pause A, Sonenberg N. 1995. The translation initiation factor eIF-4E binds to a common motif shared by the translation factor eIF-4γ and the translational repressors 4E-binding proteins. *Mol Cell Biol* **15:** 4990–4997. doi:10.1128/MCB.15.9.4990

Marcotrigiano J, Gingras AC, Sonenberg N, Burley SK. 1999. Cap-dependent translation initiation in eukaryotes is regulated by a molecular mimic of eIF4G. *Mol Cell* **3:** 707–716. doi:10.1016/S1097-2765(01)80003-4

Mayya VK, Flamand MN, Lambert AM, Jafarnejad SM, Wohlschlegel JA, Sonenberg N, Duchaine TF. 2021. microRNA-mediated translation repression through GYF-1 and IFE-4 in *C. elegans* development. *Nucleic Acids Res* **49:** 4803–4815. doi:10.1093/nar/gkab162

McCoy AJ, Grosse-Kunstleve RW, Adams PD, Winn MD, Storoni LC, Read RJ. 2007. Phaser crystallographic software. *J Appl Crystallogr* **40:** 658–674. doi:10.1107/S0021889807021206

McPhillips TM, McPhillips SE, Chiu H-J, Cohen AE, Deacon AM, Ellis PJ, Garman E, Gonzalez A, Sauter NK, Phizackerley RP, et al. 2002. Blu-ice and the distributed control system: software for data acquisition and instrument control at macromolecular crystallography beamlines. *J Synchrotron Radiat* **9:** 401–406. doi:10.1107/S0909049502015170

Mishima Y, Fukao A, Kishimoto T, Sakamoto H, Fujiwara T, Inoue K. 2012. Translational inhibition by deadenylation-independent mechanisms is central to microRNA-mediated silencing in zebrafish. *Proc Natl Acad Sci* **109:** 1104. doi:10.1073/pnas.1113350109

Moran Y, Praher D, Fredman D, Technau U. 2013. The evolution of microRNA pathway protein components in cnidaria. *Mol Biol Evol* **30:** 2541–2552. doi:10.1093/molbev/mst159

Morita M, Ler LW, Fabian MR, Siddiqui N, Mullin M, Henderson VC, Alain T, Fonseca BD, Karashchuk G, Bennett CF, et al. 2012. A novel 4EHP-GIGYF2 translational repressor complex is essential for mammalian development. *Mol Cell Biol* **32:** 3585–3593. doi:10.1128/MCB.00455-12

Nishizawa K, Freund C, Li J, Wagner G, Reinherz EL. 1998. Identification of a proline-binding motif regulating CD2-triggered T lymphocyte activation. *Proc Natl Acad Sci* **95:** 14897. doi:10.1073/pnas.95.25.14897

Peter D, Igreja I, Weber R, Wohlbold L, Weiler C, Ebertsch L, Weichenrieder O, Izaurralde E. 2015. Molecular architecture of 4E-BP translational inhibitors bound to eIF4E. *Mol Cell* **57:** 1074–1087. doi:10.1016/j.molcel.2015.01.017

Peter D, Weber R, Sandmeir F, Wohlbold L, Helms S, Bawankar P, Valkov E, Igreja C, Izaurralde E. 2017. GIGYF1/2 proteins use auxiliary sequences to selectively bind to 4EHP and repress target mRNA expression. *Genes Dev* **31:** 1147–1161. doi:10.1101/gad.299420.117

Peter D, Ruscica V, Bawankar P, Weber R, Helms S, Valkov E, Igreja C, Izaurralde E. 2019. Molecular basis for GIGYF–Me31B complex assembly in 4EHP-mediated translational repression. *Genes Dev* **33:** 1355–1360. doi:10.1101/gad.329219.119

Rom E, Kim HC, Gingras A-C, Marcotrigiano J, Favre D, Olsen H, Burley SK, Sonenberg N. 1998. Cloning and characterization of 4EHP, a novel mammalian eIF4E-related cap-binding protein. *J Biol Chem* **273:** 13104–13109. doi:10.1074/jbc.273.21.13104

Ruscica V, Bawankar P, Peter D, Helms S, Igreja C, Izaurralde E. 2019. Direct role for the *Drosophila* GIGYF protein in 4EHP-mediated mRNA repression. *Nucleic Acids Res* **47:** 7035–7048. doi:10.1093/nar/gkz429

Satterstrom FK, Kosmicki JA, Wang J, Breen MS, De Rubeis S, An J-Y, Peng M, Collins R, Grove J, Klei L, et al. 2020. Large-scale exome sequencing study implicates both developmental and functional changes in the neurobiology of autism. *Cell* **180:** 568–584.e523. doi:10.1016/j.cell.2019.12.036

Schopp IM, Amaya Ramirez CC, Debeljak J, Kreibich E, Skribbe M, Wild K, Béthune J. 2017. Split-BioID a conditional proteomics approach to monitor the composition of spatiotemporally defined protein complexes. *Nat Commun* **8:** 15690. doi:10.1038/ncomms15690

Sinha NK, Ordureau A, Best K, Saba JA, Zinshteyn B, Sundaramoorthy E, Fulzele A, Garshott DM, Denk T, Thoms M, et al. 2020. EDF1 coordinates cellular responses to ribosome collisions. *Elife* **9:** e58828. doi:10.7554/eLife.58828

Sonenberg N, Hinnebusch AG. 2009. Regulation of translation initiation in eukaryotes: mechanisms and biological targets. *Cell* **136:** 731–745. doi:10.1016/j.cell.2009.01.042

Thyme SB, Pieper LM, Li EH, Pandey S, Wang Y, Morris NS, Sha C, Choi JW, Herrera KJ, Soucy ER, et al. 2019. Phenotypic landscape of schizophrenia-associated genes defines candidates and their shared functions. *Cell* **177:** 478–491.e420. doi:10.1016/j.cell.2019.01.048

Tollenaere MAX, Tiedje C, Rasmussen S, Nielsen JC, Vind AC, Blasius M, Batth TS, Mailand N, Olsen JV, Gaestel M, et al. 2019. GIGYF1/2-driven cooperation between ZNF598 and TTP in posttranscriptional regulation of inflammatory signaling. *Cell Rep* **26:** 3511–3521.e3514. doi:10.1016/j.celrep.2019.03.006

Weber R, Chung M-Y, Keskeny C, Zinnall U, Landthaler M, Valkov E, Izaurralde E, Igreja C. 2020. 4EHP and GIGYF1/2 mediate translation-coupled messenger RNA decay. *Cell Rep* **33:** 108262. doi:10.1016/j.celrep.2020.108262

Williams CJ, Headd JJ, Moriarty NW, Prisant MG, Videau LL, Deis LN, Verma V, Keedy DA, Hintze BJ, Chen VB, et al. 2018. MolProbity: more and better reference data for improved all-atom structure validation. *Protein Sci* **27:** 293–315. doi:10.1002/pro.3330

Zou L, Moch C, Graille M, Chapat C. 2022. The SARS-CoV-2 protein NSP2 impairs the silencing capacity of the human 4EHP-GIGYF2 complex. *iScience* **25:** 104646. doi:10.1016/j.isci.2022.104646

Molecular basis for GIGYF–TNRC6 complex assembly

Meghna Sobti, Benjamin J. Mead, Alastair G. Stewart, et al.

RNA 2023 29: 724-734 originally published online February 28, 2023
Access the most recent version at doi:10.1261/rna.079596.123